Scalable electronic readout design for a 100 ps coincidence time resolution TOF-PET system

Shirin Pourashraf[1], **Andrea Gonzalez-Montoro**[1], **Jun Yeon Won**[2], **Min Sun Lee**[3], **Joshua W Cates**[1,4], **Zhixiang Zhao**[5], **Jae Sung Lee**[2], **Craig S Levin**[1,6,7,8]

[1]Department of Radiology, Molecular Imaging Program, School of Medicine, Stanford University, CA, United States of America

[2]Department of Nuclear Medicine and Biomedical Sciences, Seoul National University College of Medicine, Seoul, 110-744, Republic of Korea

[3]Nuclear Emergency & Environmental Protection Division, Korea Atomic Energy Research Institute, Daejeon, Republic of Korea

[4]Applied Nuclear Physics Program, Lawrence Berkeley National Laboratory, CA, United States of America

[5]School of Biomedical Engineering, Shanghai Jiao Tong University, Shanghai, People's Republic of China

[6]Department of Physics, Stanford University, CA, United States of America

[7]Department of Electrical Engineering, Stanford University, CA, United States of America

[8]Department of Bioengineering, Stanford University, CA, United States of America

Abstract

We have developed a scalable detector readout design for a 100 ps coincidence time resolution (CTR) time of flight (TOF) positron emission tomography (PET) detector technology. The basic scintillation detectors studied in this paper are based on 2×4 arrays of $3 \times 3 \times 10$ mm^3 'fast-LGSO:Ce' scintillation crystals side-coupled to 6×4 arrays of 3×3 mm^2 silicon photomultipliers (SiPMs). We employed a novel mixed-signal front-end electronic configuration and a low timing jitter Field Programming Gate Array-based time to digital converter for data acquisition. Using a ^{22}Na point source, >10 000 coincidence events were experimentally acquired for several SiPM bias voltages, leading edge time-pickoff thresholds, and timing channels. CTR of 102.03 ± 1.9 ps full-width-at-half-maximum (FWHM) was achieved using single $3 \times 3 \times 10$ mm^3 'fast-LGSO' crystal elements, wrapped in Teflon tape and side coupled to a linear array of 3 SiPMs. In addition, the measured average CTR was 113.4 ± 0.7 ps for the side-coupled 2×4 crystal array. The readout architecture presented in this work is designed to be scalable to large area module detectors with a goal to create the first TOF-PET system with 100 ps FWHM CTR.

cslevin@stanford.edu .

Keywords

positron emission tomography; coincidence time resolution; time-of-flight; scintillation crystal; silicon photomultipliers; front-end electronics; FPGA-based TDC

1. Introduction

Positron emission tomography (PET) imaging exploits the coincidence detection of 511 keV annihilation photon pairs to infer their origin along lines of response (LOR) between scintillation crystal elements in the system detector ring. In conventional PET imaging, the origin of these 511 keV photons can be anywhere along the LOR. Thus, during image reconstruction, the counts are evenly distributed, propagating uncertainty and noise throughout the image (Vaquero and Kinahan 2015). In time-of-flight (TOF)-PET imaging, annihilation event origins along LORs are more precisely constrained along system LORs using the 511 keV photon arrival time difference in each pair. In this case, the estimation uncertainty follows a normal distribution with full-width at half maximum (FWHM), related to the system coincidence time resolution (CTR). Including TOF information into PET image reconstruction provides enhancements in image signal-to-noise ratio (SNR) and thereby effective sensitivity. This enhanced effective sensitivity can enable better lesion detection and quantification, or optionally lower radiation dose or scanning duration (Turkington and Wilson 2009, Conti 2011, Fakhir et al 2011, Daube-Witherspoon et al 2014, Surti and Karp 2016), or a selected mixture of all three benefits. To date, the best CTR achieved by a state-of-the-art commercial TOF-PET scanner is ~214 ps FWHM at system level (Siemens Biograph Vision Technical Sheet 2019), which constrains events to a ~3.2 cm segment along LORs during image reconstruction. Achieving 100 ps FWHM CTR would constrain events to a 1.5 cm segment along each LOR, enabling a ~5-fold improvement compared to non-TOF systems and ~2-fold SNR improvement relative to the Siemens Biograph PET scanner, assuming a 40 cm diameter imaging subject.

To achieve 100 ps FWHM CTR, we have developed an innovative scintillation detector configuration (Cates and Levin 2018) that is coupled to a novel front-end electronics and data acquisitions system scheme having very low timing jitter in combination with optimized signal processing techniques (Gola et al 2011, 2012). To achieve this level of performance, front-end readouts can be assembled using high-performance analog and digital integrated circuits in combination with data acquisition systems that include time-to-digital converters (TDCs) with precise timing information (low jitter) implemented on a highly integrated field programming gate array (FPGA) (Won and Lee 2018).

In this work, we build upon a previously demonstrated 'side-readout' TOF-PET detector concept (Levin 2002), which has been demonstrated to be capable of achieving ~100 ps FWHM CTR for long (20 cm) scintillation crystal elements (Cates and Levin 2018). We evaluate an electronic readout architecture, which has been designed to facilitate scaling this side-readout detector concept to large area detector modules. The front-end electronic design includes a high speed amplifier, signal differentiator, and a NINO ASIC (Anghinolfi et al 2004), used as a fast comparator for time pickoff. The electronic readout was evaluated in

both single crystal element coincidence studies and measurements between two arrays of the same scintillation crystal elements.

2. Materials and methods

2.1. Crystal to photosensor coupling

To provide adequate detection efficiency for 511 keV annihilation photons and high spatial resolution in current clinical PET scanners, long and narrow lutetium oxyorthosilicate- (LSO)-based crystals ($\geqslant$ 20 mm length and 3 or 4 mm width) are used. A dominant factor in achievable CTR for an LSO-based detector is scintillation light photon statistics. It has previously been shown that coupling scintillation crystal elements on their long side (figure 1(b)), as opposed to the traditional coupling configuration on a crystal's narrow end (figure 1(a)), enables near-complete light collection efficiency independent of interaction depth, and also reduces the transit time jitter of scintillation light photons in their potential paths to the photodetector (Levin 2002, Cates et al 2017, Cates and Levin 2016). Less than 100 ps CTR has been achieved with $2 \times 2 \times 20$ mm^3 LYSO crystal elements coupled to the center of 4×4 mm^2 SiPM pixels where the SiPM is most sensitive (Gundacker et al 2019). However, in a practical PET system comprising arrays of crystal elements, the crystal element width should match the SiPM width, otherwise there would be relatively large gaps between elements that would reduce crystal packing fraction.

Side readout of 20 mm length fast-LGSO has achieved just above 100 ps FWHM CTR with simple leading edge time pickoff (Cates and Levin 2018). Therefore, side readout of long crystals enables an immediate pathway for clinically-relevant TOF-PET detectors capable of 100 ps FWHM CTR, and we employ this technique with a goal to achieve 100 ps FWHM CTR with a readout architecture suitable for scaling this concept from single side-coupled detector layers to large area detector modules (see figure 2) used to build a full 100 ps CTR TOF-PET system. Note that in this work, which is at the detector layer level (figure 2(a)), no specific multiplexing method is applied for energy signal; each of three adjacent SiPMs' standard output are connected together. Also, each timing channel is built by connecting three adjacent SiPMs' fast output. This leads to 8-timing signals per detector layer which are processed with one 8-channel NINO ASIC. Before transition to the sub-module (figure 2(b)), these 8-timing signals will be merged by a high performance summation component, which results in only one timing signal.

2.2. Single scintillation photon detection sensitivity

The single photon charge spectrum (SPCS) gives an indication of a scintillation detector's ability to measure pulse height of individual scintillation photons arriving at the SiPM. A detector that can differentiate the first few photoelectron peaks arriving at the photodetector above noise is a necessary (but not sufficient) ingredient for achieving good CTR (e.g. see Spanoudaki and Levin 2011).

To assess SPCR of the prototype TOF-PET readout electronics, one of the detectors shown in figure 3(b) was used. Using a 20 Gsa s^{-1}, 2 GHz Agilent DSO90254A oscilloscope, the amplified timing signal was monitored and a very low threshold voltage just above the noise

level was applied to see the distribution of the peaks, which indicates events with different number of detected photons, labeled by the number of photoelectrons (pe) detected, e.g. 1 pe, 2 pe, etc.

2.3. Prototype detector front-end readout and data acquisition electronics

Figure 3 shows a schematic and printed circuit boards (PCBs) prototypes of both front-end readout electronics and back-end data acquisition for the experimental setup used to evaluate CTR performance of the prototype TOF-PET detectors. In this experimental configuration, two identical proof-of-concept PET detector elements were assembled using two different configurations, namely: (i) $3 \times 3 \times 10$ mm^3 LGSO:Ce scintillation crystal elements (Oxide, Yamanashi, Japan 2020) wrapped with Teflon tape and side-coupled by means of optical grease (BC-640, Saint-Gobain 2020) to a 6×4 array of 3×3 mm^2 SiPMs (OnSemiconductor J-series SiPM Sensors datasheet 2018)(figure 3(b)) and; (ii) 2×4 arrays of $3 \times 3 \times 10$ mm^3 LGSO:Ce crystal elements coupled to the same SiPM array as shown in figure 3(c), to evaluate the CTR performance of the prototype detector layer. All scintillation pixels in the 2×4 LGSO: Ce arrays are chemically etched and coated with 260 μm thick BaSO$_4$ reflector (all faces except the one in contact with the photosensor). This configuration of two rows of 10 mm crystals creates an effective crystal length of 20 mm (see figure 3(c)) needed for clinical PET systems.

As shown in figure 3(a), signals derived from the AC-coupled, 'fast output' of SiPMs are used for time pickoff. These signals were first connected to a Minicircuits MAR-6 RF amplifier and then, to a balun transformer (Macom MABA-007159) with a 50 Ω impedance and 1:1 turn ratio, to generate the differential signals in an unbalanced-to-balanced configuration. The differential amplified fast outputs were connected to an 8-channel NINO ASIC (CERN, European Organization for Nuclear Research). For these studies, we use the NINO simply as a high-speed, multi-channel comparator for its moderate power consumption and a small footprint (Anghinolfi et al 2004, Nemallapudi et al 2015). In future designs, this can be replaced by any comparator with suitable performance.

The NINO digitizes timing signals from the photosensor to provide differential timing signals (compatible with Low Voltage Differential Signaling (LVDS) receivers) that are required as the input for the FPGA-based TDC. The modern FPGA boards have many (up to 1500) configurable I/O ports that can be configured to function as voltage comparators without undesirable offset voltage. This feature makes them a suitable choice for applications like our TOF-PET detector that requires multichannel digitizers and signal readout (Becker et al 2015, Won and Lee 2018). This not only increases the maximum performance of the scanner but also helps to have a highly compact and low power back-end electronic system. Therefore, in this work, we are using a very low intrinsic jitter $\sigma = 6.7$ ps (15.8 ps FWHM) FPGA-based TDC (Won and Lee 2018) design that has been adapted to our multichannel prototype TOF-PET scanner and implemented on Kintex®−7 FPGA KC705 evaluation kit including an XC7K325T-2FFG900C FPGA (figure 3(b)).

For energy measurement of each event, time-over-threshold (ToT) (Grant and Levin 2014) was implemented using the FPGA-based LVDS input receivers (Hansen and Shi 2007, Xi et al 2013, Palka et al 2017, Zhao et al 2017). Therefore, the energy signal (standard output

of the SiPMs) and the threshold voltage were directly fed into the positive and negative sides of the LVDS interface, respectively. The positive input of these LVDS interfaces were terminated to the ground using a 50 Ω resistor (Won and Lee 2018). A common FPGA energy threshold (E_{th}) was applied to negative input of LVDS interfaces of all energy channels. Several E_{th} values were swept through to find the optimal threshold value for these FPGA interfaces as a function of the SiPM biasing. The ToT values were measured using the TDC, and converted into the energy value. In order to calibrate the nonlinearity of ToT curves for the two detectors, events were acquired within an energy window of 303 to 662 keV using ^{133}Ba, ^{22}Na, and ^{137}Cs sources.

Note that for this proof-of-concept work, timing and energy signals of both detectors are connected to the FPGA by means of a custom designed add-on-board (figure 3(b)).

2.4. CTR evaluation

To evaluate CTR performance of our proof-of-concept TOF-PET detector readout, a 11.86 μCi ^{22}Na point-source was placed between two identical detectors for each of the aforementioned configurations (figures 3(b) and (c)). A total of 10 240 coincidence events were collected for each condition, and then processed using the FPGA-based TDC. The error bars of our results were estimated as the standard deviation over three measurement trials. A dark box was used to shield the detectors from ambient light. No thermal regulation was used and the room temperature remained constant at 27 °C. To determine the optimal measurement conditions, data were acquired for several SiPM bias voltages from 30.5 to 32 V with 0.5 V step size and differential NINO thresholds $V_{th} = (V_{th}^+ - V_{th}^-)$ from 150 to 500 mV with 50 mV step size (where negative NINO threshold V_{th}^- is fixed at 1.25 V).

The robustness of our front end electronics has been also initially evaluated by evaluating the CTR values over randomly chosen different channels of the NINO ASIC at optimum SiPM biasing voltage. Since the current version of the experimental setup (figure 3) does not allow us to monitor each NINO channel's output individually, another coincidence setup shown in figure 4 was used. Note this design is not as integrated as the current version shown in figure 3.

3. Experimental results

3.1. Single scintillation photon detection sensitivity

As depicted in figure 5, six photoelectron (pe) peaks above noise are distinguished in the SPCS. The peak separation and height of each peak seen are the different number of scintillation photons arriving at the SiPM, and their probability of arrival, respectively. As explained in section 2.2, this observed separation of peaks is a necessary (but not sufficient) indication that we can achieve good CTR performance for the proposed detector design (Spanoudaki and Levin 2011).

3.2. Coincidence time and energy resolution performance

Figure 6(a) summarizes the CTR values of our design as a function of different SiPM bias voltages and NINO thresholds. An average CTR value of 102.03 ± 1.9 ps at positive NINO

threshold of $V_{th}^+ = 1.45$ V was achieved for optimum SiPM biasing of 31.5 V, and FPGA energy threshold of $E_{th} = 0.45$ V. At these optimum voltages, figure 6(b) shows the best obtained coincidence time spectra with a CTR value of 99.36 ps and also the raw TOT energy spectra of the two coincidence detectors using TOT method. Energy resolutions of 14.7% and 12.9% at 511 keV were obtained for the two detectors (figure 7) after performing calibration on their corresponding TOT spectra.

Furthermore, similar experiments were performed (using experimental setup shown in figure 3(c)) to measure the CTR of 2×4 arrays of $3 \times 3 \times 10$ mm^3 fast LGSO. For three different measurements using each pixel in the array, the average CTR obtained for the whole array was 113.4 ± 0.7 ps FWHM, achieved at positive NINO threshold of 1.45 V and optimum SiPM biasing value for the $BaSO_4$ treatment, which was also determined to be 31.5 V (figure 8). Notice that CTR trend in figure 8 differs from the ones reported in figure 6. This is due to the presence of cross talk in array, and also the use of different reflectors ($BaSO_4$ for crystal arrays and Teflon tape for single crystals) which slightly change timing signal properties and result in different sensitivity to NINO threshold.

3.3. Sensitivity of results over different NINO channels

Figure 9 shows CTR values measured over several different channels of the NINO ASIC at 31.5 V bias voltage. An average CTR value of 110 ± 2ps FWHM was achieved confirming the robustness of our results over different NINO channels.

4. Discussion

The main goal of this work was to design and evaluate a scalable readout architecture for a TOF-PET detector capable of achieving 100 ps FWHM CTR using side-coupled $3 \times 3 \times 10$ mm^3 crystals. Using the described experimental setup, coincidence data were acquired for several SiPM bias voltages and NINO thresholds, achieving an average CTR of 102.03 ± 1.9 ps FWHM (figure 6(a)) for individual crystals and 113.4 ± 0.7 ps for the array. At positive NINO threshold of $V_{th}^+ = 1.45$ V, for an optimum SiPM bias voltage of 31.5 V, and with FPGA energy threshold $E_{th} = 0.45$ V. Owing to scintillation light crosstalk, the CTR value for the 2×4 array was systematically worse than that achieved with individual crystals, and can likely be further improved by optimizing the reflector material applied to the crystal surface and the coupling mechanism to the photosensor. We are currently optimizing these aspects of the detector design, which will be presented in future work.

Furthermore, CTR values were found to consistent over different NINO channels (figure 9) with standard deviation of less than 2–3 ps, a first indication of insensitivity of results over different electronic channels of our signal processing scheme.

We are currently scaling this side-coupled detector architecture (see figure 1) up to large area detector modules, as depicted in figure 2. In addition to further optimizing reflector materials and crystal array design, the FPGA-based TDC will be scaled to implement up to 64 LVDS timing & 32 energy channels to fully read the information from large area detector modules (figure 2) with signal multiplexing strategies. In the final design of the front-end

electronics and back end digital channels will be integrated in a carefully designed compact and high speed PCB board. Ultimately, we aim to demonstrate the performance of these novel detector modules in a prototype PET ring.

5. Summary and conclusion

We have evaluated the CTR performance of an innovative prototype TOF-PET detector design with a novel signal processing chain that achieves CTR values of 102.03 ± 1.9 ps FWHM (figure 6(a)) and 113.4 ± 0.7 ps FWHM (figure 8) for single pixel and array measurements, respectively. Along these measurements, the best CTR value of 99.36 ps was measured. To our knowledge, this is the first demonstration of a scalable electronic readout and detector concept to reach near 100 ps CTR with appropriate crystal element dimensions: 20 mm effective length elements where their width (3 mm) matches the dimensions of the SiPM (3 mm) in order to enable detectors with high crystal packing fraction. The robustness of the electronic readout was also demonstrated, achieving similar CTR values across different NINO channels.

Acknowledgments

References

Anghinolfi F, Jarron P, Martemiyanovb AN, Usenkoc E, Wenningera H, Williamsd MCS and Zichichide A 2004 NINO: an ultra-fast and low-power front-end amplifier/discriminator asic designed for the multigap resistive plate chamber Nucl. Instrum. Methods Phys. Res. A 533 183–7

Becker R, Casella C, Dissertori G, Fischer J, Howard A, Jeitler A, Lustermann W, Roeser U, Wang Q and Weber B 2015 The SAFIR project: an innovative high rate preclinical PET/MR detector towards dynamic multimodal imaging EJNMMI Phys. 2 A15 [PubMed: 26956270]

Cates JW, Bieniosek MF and Levin CS 2017 Highly multiplexed signal readout for a time-of-flight positron emission tomography detector based on silicon photomultipliers J. Med. Imaging 4 011012

Cates JW and Levin CS 2016 Advances in coincidence time resolution for PET Phys. Med. Biol 61 2255–65 [PubMed: 26914187]

Cates JW and Levin CS 2018 Evaluation of a clinical TOF-PET detector design that achieves 100 ps coincidence time resolution Phys. Med. Biol 63 115011 [PubMed: 29762136]

Conti M 2011 Focus on time-of-flight PET: the benefits of improved time resolution Eur. J. Nucl. Med. Mol. Imaging 38 1147–57 [PubMed: 21229244]

Daube-Witherspoon ME, Surti S, Perkins AE and Karp JS 2014 Determination of accuracy and precision of lesion uptake measurements in human subjects with time-of-flight PET J. Nucl. Med 55 602–7 [PubMed: 24604909]

Fakhir GE, Surti S, Sheuermann J and Karp JS 2011 Improvement in lesion detection with whole body oncologic TOF-PET J. Nucl. Med 52 347–53 [PubMed: 21321265]

Gola A, Piemonte C and Tarolli A 2011 Analog circuit for timing measurements with large area SiPMs coupled to LYSO crystals IEEE NSS MIC Conf. Record pp 725–31

Gola A, Piemonte C and Tarolli A 2012 The DLED algorithm for timing measurements on large area SiPMs coupled to scintillators IEEE Trans. Nucl. Sci 59 358–65

Grant AM and Levin CS 2014 A new dual threshold time-over-threshold circuit for fast timing in PET Phys. Med. Biol 59 3421–9 [PubMed: 24889105]

Gundacker S, Turtos RM, Auffray E, Paganoni M and Lecoq P 2019 High-frequency SiPM readout advances measured coincidence time resolution limits in TOF-PET Phys. Med. Biol 64 055012 [PubMed: 30630146]

Hansen WS and Shi Z 2007 ADC and TDC Implemented Using FPGA Proc IEEE Nucl. Sci. Symp. Conf. Record pp 281–6

Levin CS 2002 Design of a high-resolution and high-sensitivity scintillation crystal array for PET with nearly complete light collection IEEE Trans. Nucl. Sci 49 2236–43

Nemallapudi MV, Gundacker S, Lecoq P, Auffray E, Ferri A, Gola A and Piemonte C 2015 Sub-100 ps coincidence time resolution for positron emission tomography with LSO:Ce codoped with Ca Phys. Med. Biol 60 4635–49 [PubMed: 26020610]

On Semiconductor J-series SiPM Sensors datasheet (2018) (Publication Order Number: MICROJ–SERIES/D, December, 2018 – Rev. 6, © Semiconductor Components Industries, LLC, 2017) (https://onsemi.com/pub/Collateral/MICROJ-SERIES-D.PDF)

Pafka M et al. 2017 Multichannel FPGA based MVT system for high precision time (20 ps RMS) and charge measurement J. Instrum 12 P08001

Siemens Biograph Vision Technical Sheet 2019 retrieved April (www.siemens-healthineers.com)

Spanoudaki VC and Levin CSCS 2011 Investigating the temporal resolution limits of scintillation detection from pixelated elements: comparison between experiment and simulation Phys. Med. Biol 56 735–56 [PubMed: 21239845]

Surti S and Karp JS 2016 Advances in time-of-flight PET Phys Med. 32 12–22 [PubMed: 26778577]

Turkington TG and Wilson JM 2009 Attenuation artifacts and time-of-flight PET 2009 IEEE Nuclear Science Symp. and Medical Imaging Conf. (Orlando, FL) 2009

Vaquero JJ and Kinahan P 2015 Positron emission tomography: current challenges and opportunities for technological advances in clinical and preclinical imaging systems Annu. Rev. Biomed. Eng 17 385–414 [PubMed: 26643024]

Won JY and Lee JS 2018 Highly integrated FPGA-only signal digitization method using single-ended memory interface input receivers for Time-of-Flight PET detectors IEEE Trans. Biomed. Circuits Syst 12 1401–9 [PubMed: 30113901]

Xi D, Kao CM, Liu W, Zeng C, Liu X and Xie Q 2013 FPGA-only MVT digitizer for TOF PET IEEE Trans. Nucl. Sci 60 3253–61

Zhao Z, Huang Q, Gong Z, Su Z, Moses WM, Xu J and Peng Q 2017 A novel readout electronics design based on 1-bit sigma-delta modulation IEEE Trans. Nucl. Sci 64 820–8
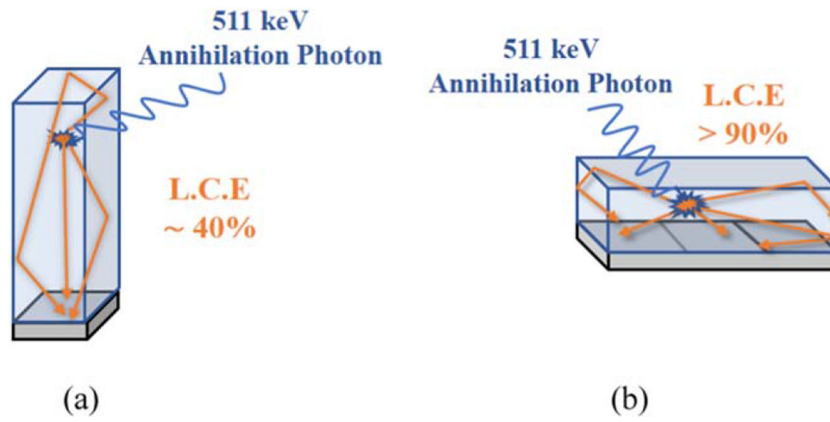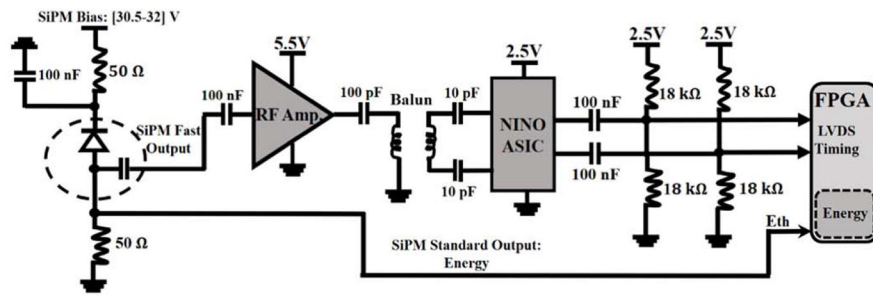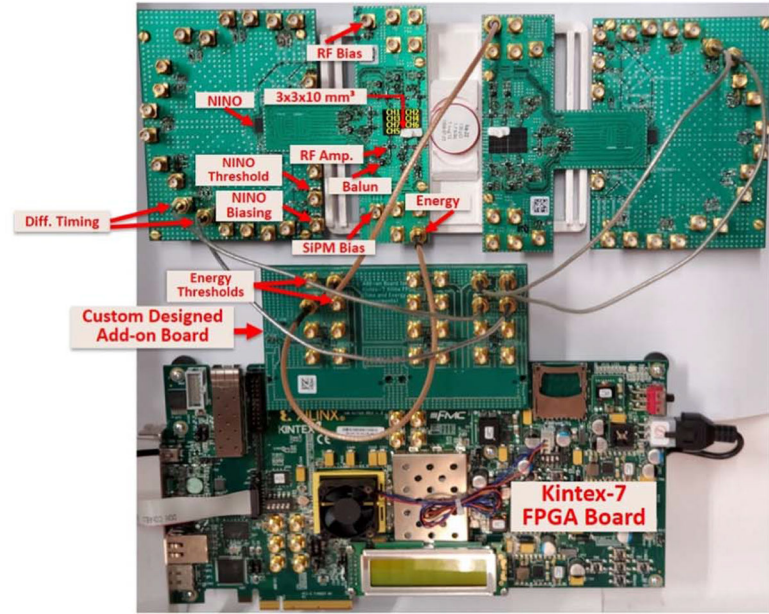
Figure 1.
Crystal to photosensor coupling: (a) Conventional end-readout configuration. (b) Side readout configuration used in this study.
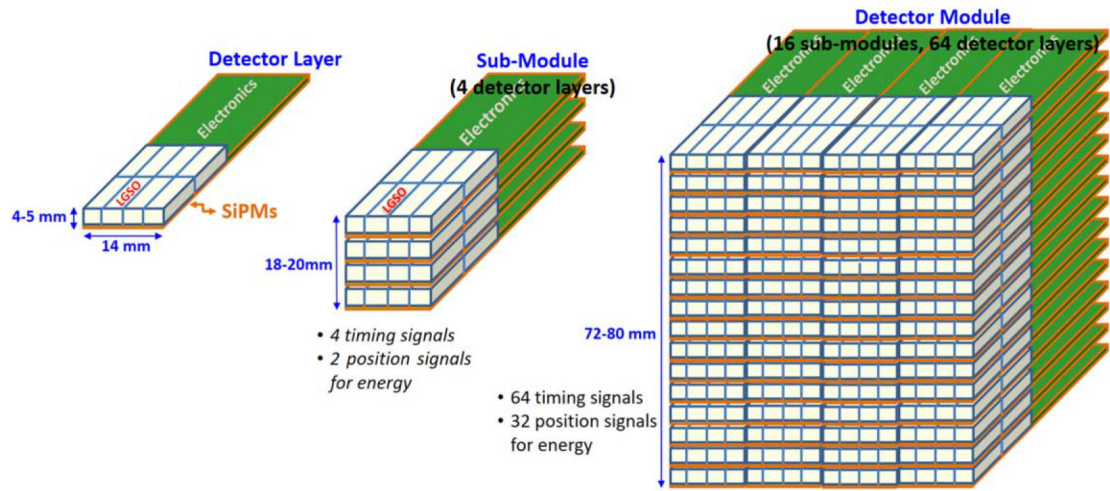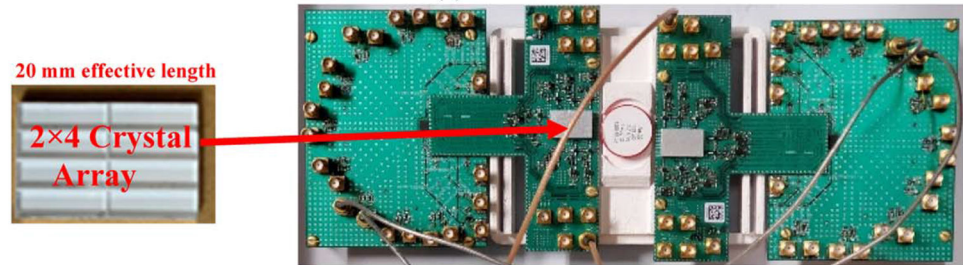
Figure 2.
Schematic of concept for a detector module that achieves ~100 ps CTR. From left to right: Single side-coupled detector layer; Sub-module, and full detector module design we employ to build a full 100 ps CTR TOF-PET system.
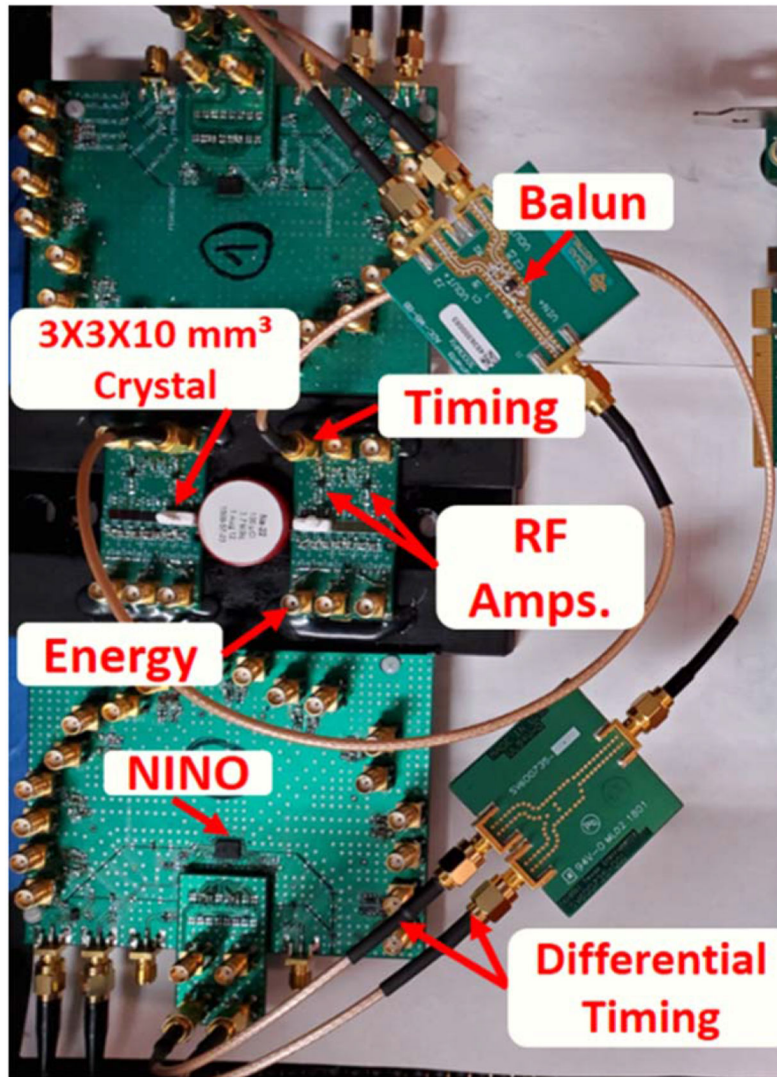
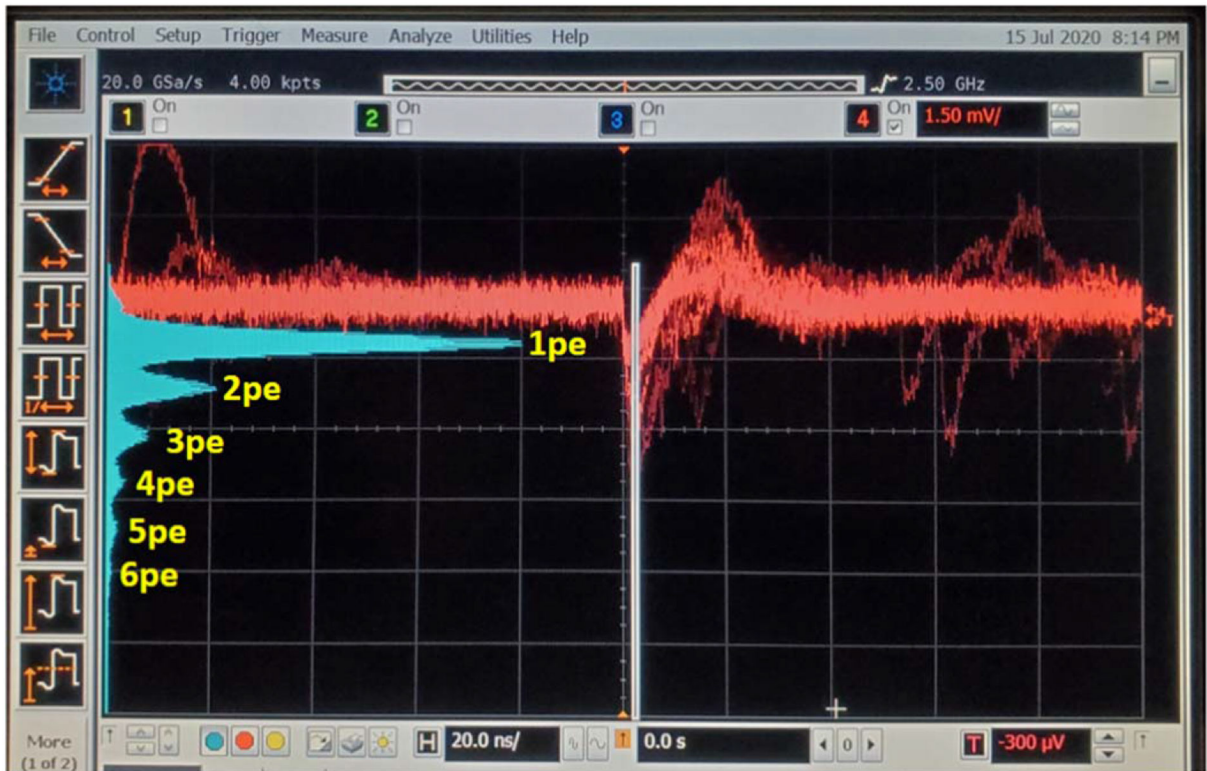**Figure 3.**
Prototype mixed-signal electronic readout and data acquisition scheme for our proposed TOF-PET detectors: (a) Schematic and (b) implementation of electronic readout and data acquisition. (c) Experimental coincidence setup using two 2×4 arrays of $3 \times 3 \times 10$ mm^3 fast-LGSO crystal elements coupled to a 6×4 array of 3×3 mm^2 SiPMs. This configuration of two rows of 10 mm crystals creates an effective crystal length of 20 mm needed for clinical PET systems.

Figure 4.
Coincidence experimental setup to enable testing the robustness of performance for different NINO channels.

Figure 5.
Single photon charge spectrum (SPCS, shown in blue) of amplified timing signal for our
prototype TOF-PET detector. The amplified timing signal is shown in red; the *x*-axis is the
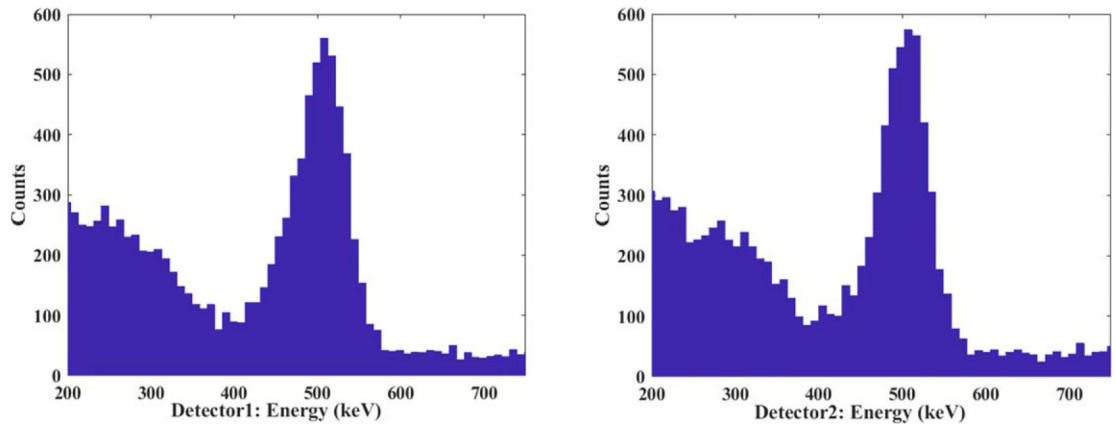time (ns) and *y*-axis is its amplitude (mV).
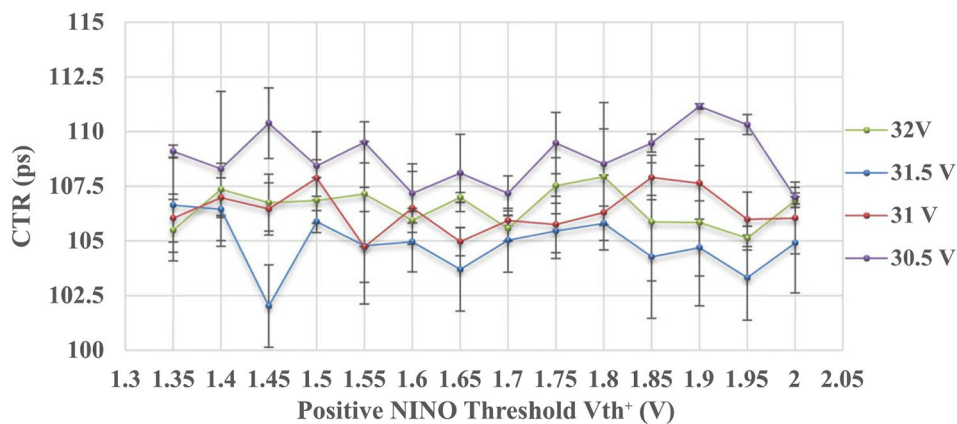
(a)
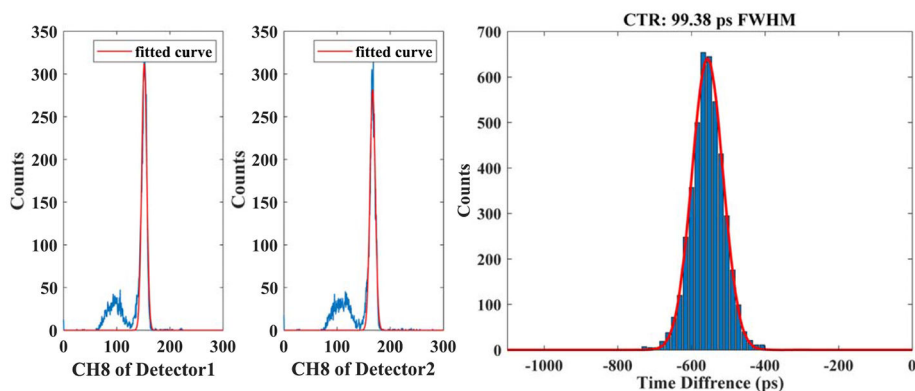
(b)

Figure 6.
(a)CTR for different SiPM bias and NINO threshold. (b) An example of detector coincidence energy spectra (left) and time spectrum (right) at positive NINO threshold of $V_{th}^{+} = 1.45$ V, optimum SiPM bias 31.5 V, and FPGA energy threshold of $E_{th} = 0.45$ V.
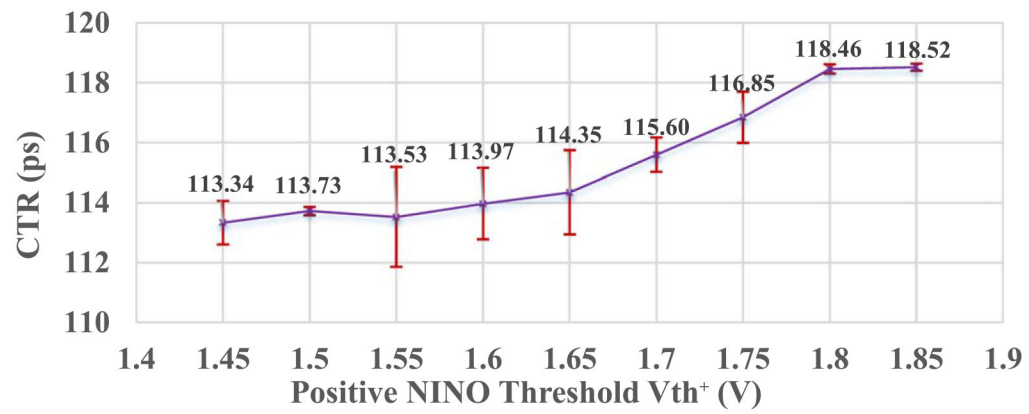
Figure 7.
Calibrated TOT-based energy spectra of the detectors (data acquired in singles mode).

Figure 8.
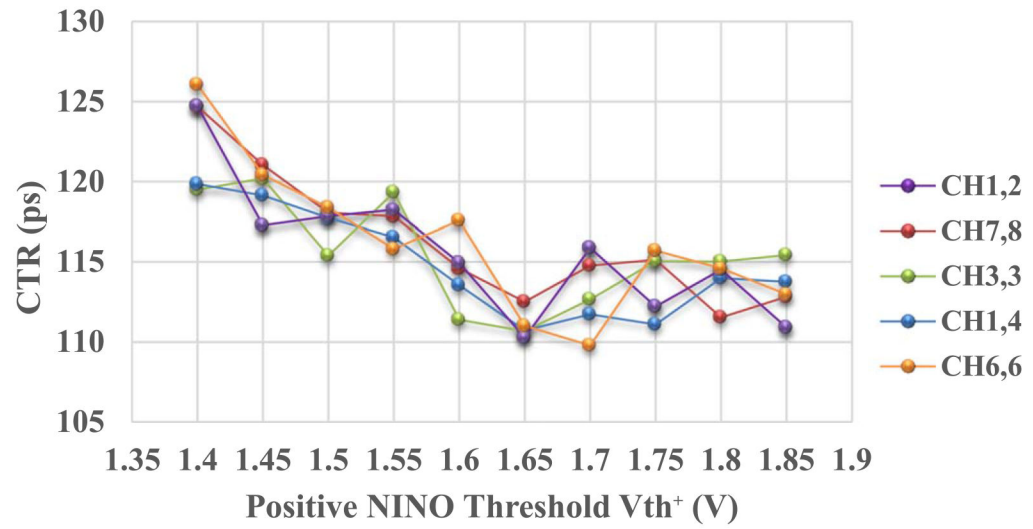Average CTR values at optimum SiPM biasing of 31.5 V and for different positive NINO thresholds achieved using 2×4 arrays of $3 \times 3 \times 10$ mm^3 chemically etched fast LGSO:Ce crystals arrays coated with 260 μm thick BaSO$_4$.

Figure 9.
CTR values across several NINO channels at 31.5 V optimum SiPM biasing. Note that 'CH$_{M,N}$' are the two NINO channels M and N used in different coincidence measurements presented.